Identification of vehicle axle loads from bridge responses using preconditioned least square QR-factorization algorithm

Zhen Chen[a,b,d*], Tommy H.T. Chan[b], Andy Nguyen[b,c], Ling Yu[d]

[a] *School of Civil Engineering and Communication, North China University of Water Resources and Electric Power, Zhengzhou 450045, China*
[b] *School of Civil Engineering and Built Environment, Queensland University of Technology (QUT), Brisbane 4000, Australia*
[c] *School of Civil Engineering of Surveying, University of Southern Queensland (USQ), Springfield Central, 4300, Australia*
[d] *MOE Key Lab of Disaster Forecast and Control in Engineering, Jinan University, Guangzhou 510632, China*

Abstract: This paper develops a novel method for moving force identification (MFI) called preconditioned least square QR-factorization (PLSQR) method. The algorithm seeks to reduce the impact of identification errors caused by unknown noise. The biaxial moving forces travel on a simply supported bridge at three different speeds is used to generate numerical simulations to assess the effectiveness and applicability of the algorithm. Results indicate that the method is more robust towards ill-posed problem and has higher identification precision than the conventional time domain method (TDM). In addition, the robustness and ill-posed immunity of PLSQR are directly affected by two kinds of regularization parameters, namely, number of iterations j and regularization matrix $\mathbf{L}$. Compared with the standard form of least square QR-factorization (LSQR), i.e., the regularization matrix $\mathbf{L}$ being the identity matrix $\mathbf{I}_n$, the PLSQR with the optimal number of iterations j and regularization matrix $\mathbf{L}$ has many advantages on MFI and it is more suitable for field trials due to better adaptability with type of sensors and number of sensors.

Keywords: moving force identification; preconditioned least square QR-factorization; time domain method; regularization parameter; preconditioner

1. Introduction

The knowledge of dynamic loads acting on bridges is always required to ensure the safety and reliability of bridges. This information on traffic loading can enable efficient and economical management of transport networks and is becoming a valuable tool for bridge safety assessment [1].

The technique of moving force identification (MFI) on bridges is to solve an inverse problem through the dynamic characteristics of vehicle-bridge system and the measured responses of bridges, which is very different from the forward problem. Force reconstruction techniques are often associated with an ill-posed problem due to the recovery of the input of a

*Corresponding author at: School of Civil Engineering and Communication, North China University of Water Resources and Electric Power, 36 Beihuan Road, Zhengzhou 450045, PR China
E-mail address: yuchenfish@163.com (Z. Chen).

dynamic system with influential noise, which leads to the reconstruction results in inaccurate or non-unique solutions [2].

There are four important indirect moving force identification methods developed by Chan et al [3-6], which have been incorporated into a moving force identification system and then evaluated by experimental verification in laboratory and field applications [7]. Comparisons show that all these four methods have acceptable accuracy; but the identification results from the time domain method (TDM) and the frequency-time domain method (FTDM) are better than those from the interpretive method I (IMI) and the interpretive method II (IMII). The TDM was widely adopted because of its high precision and rigorous theory, which can be used to identify the load history of each axle of a vehicle passing a bridge without interrupting the flow of traffic. Zhu and Law [8-10] extended the TDM to several different bridge types. Chan and Ashebo [11] extended the TDM to continuous bridge by considering the responses of only one selected span from the continuous bridge. Yu and Chan [12] proposed a method of moments (MOM) algorithm which improved the efficiency compared with the existing TDM. However, it was still found that the identification results of improved methods based on TDM suffer large deviation from real load during the local period of the vehicle crossing the bridge, since the nature of the MFI is ill-posed [13].

In the last decade, some novel techniques have been presented for MFI. Dowling et al. [14] utilized the first order regularization method to calculate the moving force from bridge strain responses. Berry et al. [15] presented the theoretical developments of identifying local dynamic transverse forces on the surface of a thin plate based on the virtual fields method. Li et al. [16] proposed a force identification algorithm based on wavelet multi-resolution analysis. Most of the new methods have noise immunity but ill-posedness should not be ignored. To overcome the ill-posedness of MFI, regularization methods used to be utilized by converting ill-posed to well-posed and these conditions can be physical or mathematical [2].

Some researchers introduced Tikhonov regularization approach to overcome ill-posedness problems in MFI, as long as the optimal regularization parameter can be correctly chosen. Pinkaew [17] adopted an updated static component (USC) technique to overcome vehicle-bridge parameter sensitivity issues such as the vehicle speed. González et al. [18] proposed a new bridge weigh in motion algorithm to reduce the dynamic uncertainty of bridge responses. Mao et al. [19] presented an improved state space method to deal with the ill-posedness problem. Ronasi et al. [20] added the traditional Tikhonov regularization method within the numerical framework to reduce the sensitivity to noise of wheel-rail contact force identification. Law et al. [21-23] proposed and an iterative regularization method for structural damping identification and damage identification when noise effect is included in the measurements. Ding et al. [24] proposed a discrete force identification approach based on average acceleration discrete algorithm. Feng et al. [25] introduced a Bayesian inference regularization to overcome the ill-posed problem for input moving loads. Qiao et al. [26,27]

proposed a regularized cubic B-spline collocation (CBSC) method to mitigate the ill-posed problem. Liu et al. [28-31] proposed a series of new methods for MFI based on Tikhonov regularization such as time-domain Galerkin method, improved regularization method and the shape function method based on moving least square fitting.

In linear algebra, the least square QR-factorization (LSQR) is an iterative method similar in style to the well-known conjugate gradients (CG) as applied to the least squares problem [32,33]. Benbow [34] extended LSQR with similar preconditioned Krylov methods for solving augmented linear systems in a generalized least squares problem. Jacobsen and Hansen [35] presented a subspace preconditioned LSQR for the solution of discrete linear ill-posed problem. Reichel et al. [36,37] presented a generalization of LSQR that allowed the choice of an arbitrary initial vector for the solution subspace. Karimi and Zali [38] proposed a block preconditioned least squares (BPLS) and a block preconditioned global least squares (BPGLS) algorithms to solve the linear system of equations with block partitioned coefficient matrix and multiple linear system of equations. Arridge et al. [39] derived a factorization-free preconditioned LSQR algorithm (MLSQR) for solving large-scale linear inverse imaging problems.

As mentioned earlier, out of many iterative methods for solving the linear algebraic equation, LSQR is a popular iterative method for the solution of large linear systems of equations and least-squares problems [36]. In this paper, based on the LSQR technique, a preconditioned least square QR-factorization (PLSQR) regularization method is proposed for MFI by choosing proper regularization parameter, such as the number of iterations and the regularization matrix. The numerical simulation results show that the PLSQR has excellent ill-posed immunity and high-quality adaptability with different sensors. These advantages of PLSQR are practical to the field trials of MFI.

2. Background of theory

2.1. Moving force identification by time domain method (TDM)

As shown in Fig.1, a moving force $f(t)$ passes over a simply supported Bernoulli-Euler beam at a constant speed c. The span of the beam is L and viscous damping is C. The mass per unit length of the beam is ρ and flexural stiffness is EI. The dynamic equation of vehicle-bridge system in modal coordinate $q_n(t)$ can be expressed as

$$\ddot{q}_n(t) + 2\xi_n\omega_n\dot{q}_n(t) + \omega_n^2 q_n(t) = \frac{2}{\rho L}p_n(t), \quad (\mathrm{n} = 1,2,\ldots,\infty) \tag{1}$$

where $\omega_n = \frac{n^2\pi^2}{L^2}\sqrt{\frac{EI}{\rho}}$ is the nth modal frequency; $\xi_n = \frac{C}{2\rho\omega_n}$ is the modal damping ratio; $p_n(t) = f(t)\sin\frac{n\pi ct}{L}$ is the modal force.

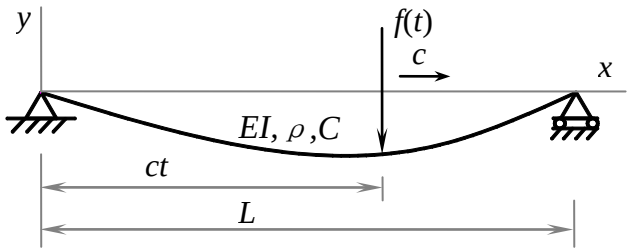

Fig.1. Dynamic model of moving vehicle and simply supported beam

The deflection $v(x,t)$ and the bending moment $M(x,t)$ of the simply supported beam at point x and time t in time domain can be obtained as Law et al. [4]

$$v(x,t)=\sum_{n=1}^{\infty}\frac{2}{\rho L\omega_n'}\sin\frac{n\pi x}{L}\int_0^t e^{-\xi_n\omega_n(t-\tau)}\sin\omega_n'(t-\tau)\sin\frac{n\pi c\tau}{L}f(\tau)d\tau \tag{2}$$

$$M(x,t)=-EI\frac{\partial^2 v(x,t)}{\partial x^2}=\sum_{n=1}^{\infty}\frac{2EI\pi^2}{\rho L^3}\frac{n^2}{\omega_n'}\sin\frac{n\pi x}{L}\int_0^t e^{-\xi_n\omega_n(t-\tau)}\sin\omega_n'(t-\tau)\sin\frac{n\pi c\tau}{L}f(\tau)d\tau \tag{3}$$

where $\omega_n'=\omega_n\sqrt{1-\xi_n^2}$.

The MFI from bending moment responses by TDM can be expressed as

$$\mathbf{B}\cdot\mathbf{f}=\mathbf{M} \tag{4}$$

where $\mathbf{B}\in\mathbf{R}^{(N-1)\times(N_B-1)}$, $\mathbf{f}\in\mathbf{R}^{(N_B-1)}$ and $\mathbf{M}\in\mathbf{R}^{(N-1)}$. Definition the time interval is Δt, the number of sample points is $N+1$ and $N_B=\frac{L}{c\Delta t}$.

Similarly, the acceleration $\ddot{v}(x,t)$ of the simply supported beam at point x and time t in time domain can be expressed as

$$\ddot{v}(x,t)=\sum_{n=1}^{\infty}\frac{2}{\rho L}\sin\frac{n\pi x}{L}\left[f(t)\sin\frac{n\pi x}{L}+\int_0^t\ddot{h}_t(t-\tau)f(\tau)\sin\frac{n\pi c\tau}{L}d\tau\right] \tag{5}$$

where $\ddot{h}_n(t)=\frac{1}{\omega_n'}e^{-\xi_n\omega_n t}\times\{[(\xi_n\omega_n)^2-\omega_n'^2]\sin\omega_n' t+(-2\xi_n\omega_n\omega_n')\cos\omega_n' t\}$.

The MFI from acceleration responses by TDM can be expressed as

$$\mathbf{A}\cdot\mathbf{f}=\ddot{\mathbf{V}} \tag{6}$$

where $\mathbf{A}\in\mathbf{R}^{N\times(N_B-1)}$, $\mathbf{f}\in\mathbf{R}^{(N_B-1)}$ and $\ddot{\mathbf{V}}\in\mathbf{R}^{N}$.

Likewise, the MFI from bending moment and acceleration combination responses by TDM can be expressed as

$$\begin{bmatrix}\mathbf{B}/\|\mathbf{M}\|\\ \mathbf{A}/\|\ddot{\mathbf{V}}\|\end{bmatrix}\times\mathbf{f}=\begin{Bmatrix}\mathbf{M}/\|\mathbf{M}\|\\ \ddot{\mathbf{V}}/\|\ddot{\mathbf{V}}\|\end{Bmatrix} \tag{7}$$

where $\|\cdot\|$ is the norm of the vector.

2.2. Theory of least square QR-factorization (LSQR)

Based on the existing TDM, the MFI dynamic equation of vehicle-bridge system can be simplified to the form $\mathbf{Ax}=\mathbf{b}$, where the $\mathbf{A}$ is large and spare matrix, the vector $\mathbf{x}$ is time-

varying force need to be identified and the vector $\mathbf{b}$ is measured dynamic responses of bridge. With bidiagonalization procedure, algorithm LSQR is acceptable of solving least-squares problems $\min\|\mathbf{Ax}-\mathbf{b}\|_2$, where $\mathbf{A}\in\mathbf{R}^{m\times n}$, $\mathbf{x}\in\mathbf{R}^{n}$, $\mathbf{b}\in\mathbf{R}^{m}$, $m\geq n$. The residual norm $\|\mathbf{r}_j\|_2$ decreases monotonically with j-step iterations, where $\mathbf{r}_j=\mathbf{b}-\mathbf{A}\mathbf{x}_j$.

The symmetric Lanczos process is adopted to solve symmetric linear equations $\mathbf{Bx}=\mathbf{b}$ with a symmetric matrix $\mathbf{B}$ and a starting vector $\mathbf{b}$. A sequence of vectors $\mathbf{v}_i,\mathbf{w}_i$ and positive scalars α_i,β_i $(i=1,2,...,)$ are introduced to make sure matrix $\mathbf{B}$ is reduced to tridiagonal form, which can be expressed as

$$\begin{aligned}\beta_1\mathbf{v}_1&=\mathbf{b}\\ \mathbf{w}_i&=\mathbf{B}\mathbf{v}_i-\beta_i\mathbf{v}_{i-1}\\ \alpha_i&=\mathbf{v}_i^T\mathbf{w}_i\\ \beta_{i+1}\mathbf{v}_{i+1}&=\mathbf{w}_i-\alpha_i\mathbf{v}_i\end{aligned}\tag{8}$$

where $\mathbf{v}_0\equiv 0$ and each $\beta_i\geq 0$ is chosen so that $\|\mathbf{v}_i\|=1(i>0)$. The solution after j-step iterations can be expressed as

$$\mathbf{B}\mathbf{V}_j=\mathbf{V}_j\mathbf{T}_j+\beta_{j+1}\mathbf{v}_{j+1}\mathbf{e}_j^T\tag{9}$$

where $\mathbf{e}_j$ is the j-th unit vector, $\mathbf{T}_j\equiv\mathrm{tridiag}(\beta_j,\alpha_j,\beta_{j+1})=\begin{bmatrix}\alpha_1 & \beta_2 & \cdots & 0 & 0\\ \beta_2 & \alpha_2 & \beta_3 & 0 & 0\\ \vdots & \ddots & \ddots & \ddots & \vdots\\ 0 & 0 & \beta_{j-1} & \alpha_{j-1} & \beta_j\\ 0 & 0 & \ldots & \beta_j & \alpha_j\end{bmatrix}$ and $\mathbf{V}_j\equiv\left[\mathbf{v}_1,\mathbf{v}_2,\ldots,\mathbf{v}_j\right]$ with $\mathbf{V}_j^T\mathbf{V}_j=\mathbf{I}$ when no rounding error included.

Multiplying Eq. (9) by an arbitrary j-vector $\mathbf{y}_j$, whose last element is η_j, the Eq. (9) can be expressed as

$$\mathbf{B}\mathbf{V}_j\mathbf{y}_j=\mathbf{V}_j\mathbf{T}_j\mathbf{y}_j+\eta_j\beta_{j+1}\mathbf{v}_{j+1}\tag{10}$$

Since $\mathbf{V}_j(\beta_1\mathbf{e}_1)=\mathbf{b}$ is defined, by defining $\mathbf{T}_j\mathbf{y}_j=\beta_1\mathbf{e}_1$ and $\mathbf{x}_j=\mathbf{V}_j\mathbf{y}_j$, then the Eq. (10) can be expressed as

$$\mathbf{B}\mathbf{x}_j=\mathbf{b}+\eta_j\beta_{j+1}\mathbf{v}_{j+1}\tag{11}$$

By defining $\|\mathbf{u}_i\|=\|\mathbf{v}_i\|=1$, $\mathbf{U}_j\equiv\left[\mathbf{u}_1,\mathbf{u}_2,\ldots,\mathbf{u}_j\right]$, $\mathbf{B}_j\equiv\begin{bmatrix}\alpha_1 & & & & \\ \beta_2 & \alpha_2 & & & \\ & \beta_3 & \ddots & & \\ & & \ddots & \alpha_{j-1} & \\ & & & \beta_{j-1} & \alpha_j\end{bmatrix}$, the results of $\min\|\mathbf{Ax}-\mathbf{b}\|_2$ can be reduced to lower bidiagonal form by Lanczos process as

$$\begin{aligned}\mathbf{U}_{j+1}(\beta_1\mathbf{e}_1)&=\mathbf{b}\\ \mathbf{A}\mathbf{V}_j&=\mathbf{U}_{j+1}\mathbf{B}_j\end{aligned}\tag{12}$$

As $\mathbf{r}_j=\mathbf{b}-\mathbf{A}\mathbf{x}_j$, $\mathbf{x}_j=\mathbf{V}_j\mathbf{y}_j$ and then the j iterative steps of Lanczos process of problem $\min\|\mathbf{Ax}-\mathbf{b}\|_2$ can be expressed as

$$\min\|\mathbf{r}_j\|_2=\min\|\mathbf{U}_{j+1}(\beta_1\mathbf{e}_1)-\mathbf{A}\mathbf{V}_j\mathbf{y}_j\|_2=\min\|\beta_1\mathbf{e}_1-\mathbf{B}_j\mathbf{y}_j\|_2\tag{13}$$

The conventional QR factorization of $\mathbf{B}_j$ can be used in Eq. (13) and then the identification moving force $\mathbf{x}_j$ by LSQR method can be obtained with j-step iterations.

2.3. Theory of preconditioned least square QR-factorization (PLSQR)

For ill-posed inverse problems, the matrix $\mathbf{A}$ is a discretization of a compact operator which singular values accumulate at zero, rendering such clustering impossible. It is possible to modify the LSQR algorithm and derive a hybrid between a direct and an iterative regularization algorithm. A preconditioned version of LSQR for the general form problem where one minimizes $\|\mathbf{Lx}\|_2$ instead of $\|\mathbf{x}\|_2$ can be realized by introducing the regularization matrix $\mathbf{L}$. Here, the matrix $\mathbf{L}$ is typically either the identity matrix $\mathbf{I_n}$ or a $p \times n$ discrete approximation of the $(n-p)$-th derivative operator, in which case $\mathbf{L}$ is a banded matrix with full row rank. If the matrix $\mathbf{L}$ is the identity matrix $\mathbf{I_n}$, then it is the standard form of LSQR. The singular value decomposition (SVD) of matrix $\mathbf{A}$ can be expressed as $\mathbf{A} = \mathbf{U\Sigma V}^T = \sum_{i=1}^{n} \mathbf{u}_i\, \boldsymbol{\sigma}_i \mathbf{v}_i^T$. Then the generalized singular value decomposition (GSVD) of the matrix pair $(\mathbf{A}, \mathbf{L})$ are the square roots of matrix pair $(\mathbf{A^TA}, \mathbf{L^TL})$, where $\mathbf{A} \in \mathbf{R}^{m\times n}$, $\mathbf{L} \in \mathbf{R}^{p\times n}$ and the constants satisfy $m \geq n \geq p$. The matrix $\mathbf{A}$ and $\mathbf{L}$ of the GSVD can be obtained as

$$\mathbf{A} = \mathbf{U}\begin{pmatrix} \mathbf{\Sigma} & 0 \\ 0 & \mathbf{I}_{n-p} \end{pmatrix}\mathbf{X}^{-1}, \quad \mathbf{L} = \mathbf{V}(\mathbf{M}, \quad 0)\mathbf{X}^{-1} \tag{14}$$

where $\mathbf{U} \in \mathbf{R}^{m\times n}$ and $\mathbf{V} \in \mathbf{R}^{p\times p}$ are orthonormal columns matrices, $\sum = \mathrm{diag}(\sigma_1, \sigma_2, \cdots, \sigma_p)$ and $\mathbf{M} = \mathrm{diag}(\mu_1, \mu_2, \cdots, \mu_p)$ are $p \times p$ non-negative diagonal elements as $1 \geq \sigma_p \geq \cdots \geq \sigma_2 \geq \sigma_1 \geq 0$, $1 \geq \mu_1 \geq \mu_2 \geq \cdots \geq \mu_p \geq 0$, $\sigma_i^2 + \mu_i^2 = 1\ (i = 1,2,\cdots,p)$, $\mathbf{X} \in \mathbf{R}^{n\times n}$ is nonsingular. The $\mathbf{A}$-weighted generalized pseudoinverse of $\mathbf{L}$ can be defined as $\mathbf{L_A^+} = \mathbf{X}\begin{pmatrix} \mathbf{M}^{-1} \\ 0 \end{pmatrix}\mathbf{V}^T$. By introducing $\bar{\mathbf{A}} = \mathbf{AL_A^+}$, $\bar{\mathbf{b}} = \mathbf{b} - \mathbf{Ax}_0$ and $\bar{\mathbf{x}} = \mathbf{Lx}$ where $\mathbf{x}_0 = \sum_{i=p+1}^{n}\left(\mathbf{u}_i^T\mathbf{b}\right)\mathbf{x}_i$, the solution of $\min\|\mathbf{Ax} - \mathbf{b}\|_2$ can be transformed into $\min\left\|\bar{\mathbf{A}}\bar{\mathbf{x}} - \bar{\mathbf{b}}\right\|_2$ by introducing preconditioner $\mathbf{L_A^+}(\mathbf{L_A^+})^T$.

Then the Krylov solvers can be used to solve the linearized regularized least squares problem.

$$\min\left\|\bar{\mathbf{A}}\bar{\mathbf{x}} - \bar{\mathbf{b}}\right\|_2 \quad \text{subject to} \quad \bar{\mathbf{x}} \in \mathcal{K}\left(\bar{\mathbf{A}}^T\bar{\mathbf{A}}, \bar{\mathbf{A}}^T\bar{\mathbf{b}}\right) \tag{15}$$

where $\mathcal{K}\left(\bar{\mathbf{A}}^T\bar{\mathbf{A}}, \bar{\mathbf{A}}^T\bar{\mathbf{b}}\right)$ is the Krylov subspace associated with the normal equations, consider the side constraint in Eq. (15) which implies that there exist constants $\xi_0, \xi_1, \cdots, \xi_{j-1}$ such that

$$\bar{\mathbf{x}}_j = \sum_{i=0}^{j-1} \xi_i (\bar{\mathbf{A}}^T\bar{\mathbf{A}})^i \bar{\mathbf{A}}^T\,\bar{\mathbf{b}} = \sum_{i=0}^{j-1} \xi_i \left((\mathbf{L_A^+})^T\mathbf{A^TAL_A^+}\right)^i (\mathbf{L_A^+})^T\,\mathbf{A^T}(\mathbf{b} - \mathbf{Ax}_0) \tag{16}$$

With $\mathbf{x}_j = \mathbf{L_A^+}\bar{\mathbf{x}}_j + \mathbf{x}_0$ and $(\mathbf{L_A^+})^T\mathbf{A^TAx}_0 = \mathbf{0}$, the j-step iterations of PLSQR can be expressed as

$$\mathbf{x}_j = \sum_{i=0}^{j-1} \xi_i \left(\mathbf{L_A^+}(\mathbf{L_A^+})^T\mathbf{A^TA}\right)^i \mathbf{L_A^+}(\mathbf{L_A^+})^T\,\mathbf{A^Tb} + \mathbf{x}_0 \tag{17}$$

3. Numerical simulation

3.1. Simulation parameters of vehicle-bridge system

Biaxial time-varying forces pass over passes over the simply supported Bernoulli-Euler beam at three different speeds. A total of 12 cases have been considered include MFI from bending moment responses alone, acceleration responses alone and combined responses as shown in the first column in Table 1. The biaxial time-varying forces are simulated as follow

$$f_1(t) = 20\,000[1 + 0.1\sin(10\pi t) + 0.05\sin(40\pi t)]\ \mathrm{N}$$
$$f_2(t) = 20\,000[1 - 0.1\sin(10\pi t) + 0.05\sin(50\pi t)]\ \mathrm{N}$$

The distance between biaxial time-varying forces is 4 m and the three decreasing moving speeds are $c_1 = 40\mathrm{m}\cdot\mathrm{s}^{-1}$, $c_2 = 30\mathrm{m}\cdot\mathrm{s}^{-1}$ and $c_3 = 20\mathrm{m}\cdot\mathrm{s}^{-1}$, respectively. The parameters of the Bernoulli-Euler beam are as follows: $L = 40\mathrm{m}$, $\rho = 12\,000\mathrm{kg}\cdot\mathrm{m}^{-1}$, $EI = 1.274916\times10^{11}\ \mathrm{N}\cdot\mathrm{m}^2$, the sampling frequency of the beam dynamic responses is 200Hz and the analysis frequency of the numerical simulation is from 0Hz to 40Hz, which contains the first three natural frequencies of the simply supported beam including 3.2Hz, 12.8Hz and 28.8Hz, respectively.

The random noise is introduced to simulate the polluted dynamic responses by the following equation

$$\mathrm{R}_{\mathrm{measured}} = \mathrm{R}_{\mathrm{calculated}}\cdot(1 + E_p\cdot\mathrm{N}_{\mathrm{noise}}) \tag{18}$$

where E_p is noise level choosing as 1%, 5% and 10% in subsequent studies; $\mathrm{N}_{\mathrm{noise}}$ is a standard normal distribution vector.

The relatively percentage error (RPE) values between the true force and the identified force are calculated to evaluate the identification accuracy of the different methods as

$$\mathrm{RPE} = \frac{\|\mathrm{f}_{\mathrm{identified}} - \mathrm{f}_{\mathrm{true}}\|}{\|\mathrm{f}_{\mathrm{true}}\|}\times 100\% \tag{19}$$

3.2. Choosing proper regularization matrix **L** *for PLSQR*

The preconditioner $\mathbf{L}_\mathbf{A}^+(\mathbf{L}_\mathbf{A}^+)^T$ is derived from regularization matrix **L** and vehicle-bridge system matrix **A**. Related research results show that the choosing of regularization matrix **L** has tremendous influence on ill-posed immunity of PLSQR, which should be scrutinized chosen by various cases in subsequent studies. In order to evaluate the effect of different regularization matrices on the identification accuracy of PLSQR method, a total of ten different matrices are considered based on the finite difference methods. The first regularization matrix $\mathbf{L}_1$ is the identity matrix $\mathbf{I}_n$, which corresponds to the standard form LSQR method since there no regularization process. The second regularization matrix $\mathbf{L}_2$ to the tenth regularization matrix $\mathbf{L}_{10}$ are corresponding to the first derivative operator of identity matrix to the ninth derivative operator of identity matrix, respectively. A combined response with one bending moment response at middle span of simply supported Bernoulli-Euler beam and two acceleration responses at a quarter and middle span of the beam are used to evaluate the effect of ten regularization matrices on the PLSQR method. The simplified form of the combined responses can be expressed as 1/2m&1/4a&1/2a and the simplified form will be adopted by default in subsequent studies.

The abscissa values are corresponding to regularization matrices $\mathbf{L}_1$ to $\mathbf{L}_{10}$ in Fig.2, respectively. The illustration results show the RPE values firstly decrease and then increase with the increase of n-th derivative operators from identity matrix to ninth derivative operators. By choosing proper regularization matrix $\mathbf{L}$, such as the $\mathbf{L}_2$, $\mathbf{L}_3$ and $\mathbf{L}_4$, the RPE values of PLSQR are much lower than LSQR without preconditioner and PLSQR with high derivative operators from $\mathbf{L}_5$ to $\mathbf{L}_{10}$. When high derivative operators are adopted as regularization matrix, the RPE values of PLSQR become higher than the those RPE values of standard form LSQR method, which indicates that the identification accuracy of PLSQR varies with different regularization matrices. The regularization matrix $\mathbf{L}$ is a $(n-p)\times n$ band matrix with full row rank where the number p is corresponding to the p-th derivative operator while the number $p+1$ is corresponding to the width of the band. As shown in the following Eq. (20), the higher order the derivative operator is adopted, the larger the width of the band is, which complicates the left and right orthogonal transformations due to less null space of regularization matrix. Moreover, the resulting sparse problem with banded matrix has effect on non-negative diagonal elements and efficacy of preconditioner. The fundamental purpose of the preconditioner $\mathbf{L}_\mathbf{A}^+(\mathbf{L}_\mathbf{A}^+)^T$ is to ensure the j iterative steps solution of PLSQR lies in the correct subspace and thus minimizes $\left\|\mathbf{L}\mathbf{x}_j\right\|_2$. With high derivative operators from $\mathbf{L}_5$ to $\mathbf{L}_{10}$, the efficacy of preconditioner is reduced leading to large RPE values of PLSQR. The regularization matrices $\mathbf{L}_1$, $\mathbf{L}_2$, $\mathbf{L}_3$, $\mathbf{L}_4$ and $\mathbf{L}_5$ are corresponding to LSQR, PLSQR($\mathbf{L}_2$), PLSQR($\mathbf{L}_3$), PLSQR($\mathbf{L}_4$) and PLSQR($\mathbf{L}_5$), respectively, which can be shown as follow

$$
\begin{aligned}
\mathbf{L}_1 &= \begin{pmatrix} 1 & & & \\ & 1 & & \\ & & \ddots & \\ & & & 1 \end{pmatrix}_{n\times n} \\
\mathbf{L}_2 &= \begin{pmatrix} -1 & 1 & & & \\ & -1 & 1 & & \\ & & \ddots & \ddots & \\ & & & -1 & 1 \end{pmatrix}_{(n-1)\times n} \\
\mathbf{L}_3 &= \begin{pmatrix} 1 & -2 & 1 & & & \\ & 1 & -2 & 1 & & \\ & & \ddots & \ddots & \ddots & \\ & & & 1 & -2 & 1 \end{pmatrix}_{(n-2)\times n}
\end{aligned}
\tag{20}
$$

$$\mathbf{L}_4=\begin{pmatrix} -1 & 3 & -3 & 1 & & & \\ & -1 & 3 & -3 & 1 & & \\ & & \ddots & \ddots & \ddots & \ddots & \\ & & & -1 & 3 & -3 & 1 \end{pmatrix}_{(n-3)\times n}$$

$$\mathbf{L}_5=\begin{pmatrix} 1 & -4 & 6 & -4 & 1 & & \\ & 1 & -4 & 6 & -4 & 1 & \\ & & \ddots & \ddots & \ddots & \ddots & \ddots \\ & & & 1 & -4 & 6 & -4 & 1 \end{pmatrix}_{(n-4)\times n}$$

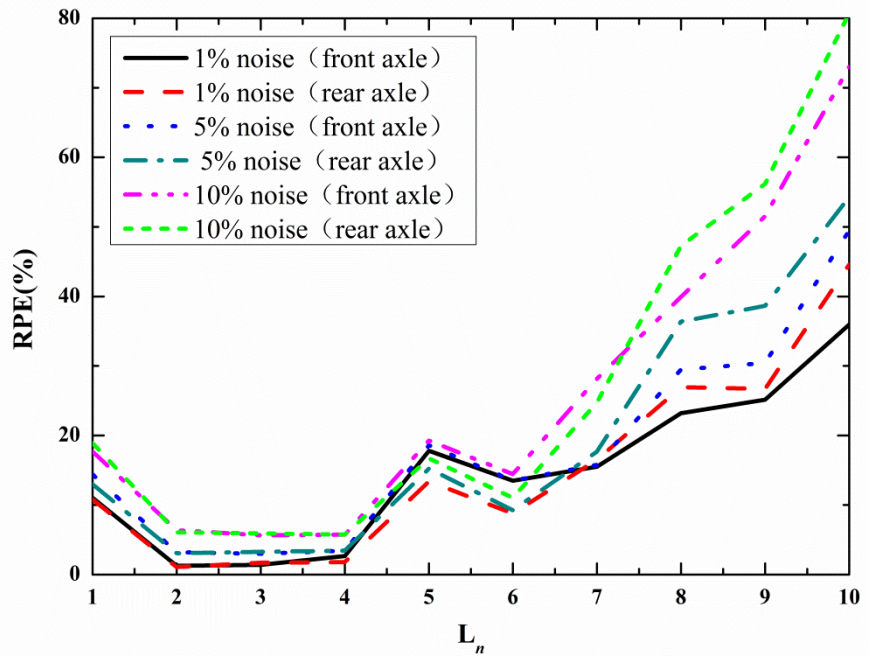

Fig.2. The RPE values identified by PLSQR with ten regularization matrices (1/2m&1/4a&1/2a)

Table 1
The RPE values (%) identified by LSQR and PLSQR with three regularization matrices

Sensor location	regularization matrix **L**	1% noise		5% noise		10% noise	
		front axle	rear axle	front axle	rear axle	front axle	rear axle
1/4m&1/2m	LSQR($\mathbf{L}_1$)	26.0	21.3	33.8	28.7	90.6	95.8
	PLSQR($\mathbf{L}_2$)	5.0	5.2	15.2	11.5	29.3	22.9
	PLSQR($\mathbf{L}_3$)	*4.6*	*4.1*	*17.6*	*9.9*	*25.7*	*19.2*
	PLSQR($\mathbf{L}_4$)	(6.3)	(4.6)	(12.3)	(9.1)	(20.5)	(16.4)
1/4m&1/2m&3/4m	LSQR($\mathbf{L}_1$)	17.1	18.9	24.2	25.3	68.7	70.2
	PLSQR($\mathbf{L}_2$)	3.3	3.1	13.9	7.6	29.3	27.4
	PLSQR($\mathbf{L}_3$)	*3.9*	*2.8*	*13.8*	*12.7*	*27.4*	*29.2*
	PLSQR($\mathbf{L}_4$)	(3.7)	(2.8)	(8.6)	(6.9)	(17.0)	(12.0)
1/4a&1/2a	LSQR($\mathbf{L}_1$)	7.4	3.2	13.3	10.3	16.8	16.4
	PLSQR($\mathbf{L}_2$)	0.5	1.2	2.8	2.9	5.4	5.6
	PLSQR($\mathbf{L}_3$)	*1.4*	*0.9*	*2.4*	*2.7*	*4.3*	*4.7*
	PLSQR($\mathbf{L}_4$)	(1.7)	(1.8)	(3.4)	(3.0)	(4.9)	(4.7)
1/4a&1/2a&3/4a	LSQR($\mathbf{L}_1$)	0.6	1.1	2.5	5.2	4.4	11.8
	PLSQR($\mathbf{L}_2$)	0.5	1.1	1.9	1.4	2.8	3.1
	PLSQR($\mathbf{L}_3$)	*0.7*	*0.9*	*1.5*	*2.5*	*2.7*	*3.9*
	PLSQR($\mathbf{L}_4$)	(1.7)	(1.4)	(1.7)	(3.1)	(2.8)	(4.1)
1/2m&1/2a	LSQR($\mathbf{L}_1$)	14.2	16.0	18.3	20.7	20.3	22.8

1/4m&1/2m&1/2a	PLSQR($\mathbf{L}_2$)	3.3	2.9	9.0	7.2	14.4	9.9
	PLSQR($\mathbf{L}_3$)	*3.2*	*3.5*	*10.2*	*7.4*	*14.9*	*9.5*
	PLSQR($\mathbf{L}_4$)	(3.8)	(4.2)	(13.4)	(13.3)	(24.5)	(18.7)
	LSQR($\mathbf{L}_1$)	14.1	15.3	18.1	20.7	21.1	23.5
	PLSQR($\mathbf{L}_2$)	2.4	3.7	8.1	9,8	14.9	11.2
	PLSQR($\mathbf{L}_3$)	*2.6*	*2.6*	*8.0*	*9.6*	*15.2*	*9.1*
	PLSQR($\mathbf{L}_4$)	(3.5)	(3.2)	(10.9)	(11.8)	(21.0)	(17.7)
1/4m&1/2m&1/4a&1/2a	LSQR($\mathbf{L}_1$)	8.2	3.1	14.9	11.3	17.8	19.3
	PLSQR($\mathbf{L}_2$)	1.4	1.4	2.8	3.0	8.2	7.8
	PLSQR($\mathbf{L}_3$)	*1.6*	*1.3*	*3.1*	*3.7*	*5.1*	*5.9*
	PLSQR($\mathbf{L}_4$)	(1.7)	(1.8)	(2.6)	(4.8)	(5.1)	(9.8)
1/4m&1/4a	LSQR($\mathbf{L}_1$)	16.0	15.2	19.4	22.9	23.7	29.7
	PLSQR($\mathbf{L}_2$)	3.7	5.5	6.2	5.2	10.9	9.3
	PLSQR($\mathbf{L}_3$)	*4.7*	*4.7*	*9.7*	*7.1*	*10.2*	*7.6*
	PLSQR($\mathbf{L}_4$)	(6.6)	(5.1)	(13.6)	(18.3)	(26.6)	(28.6)
1/4m&1/4a&1/2a	LSQR($\mathbf{L}_1$)	8.5	3.1	14.5	12.1	17.2	18.8
	PLSQR($\mathbf{L}_2$)	1.3	1.4	2.7	2.2	4.1	4.2
	PLSQR($\mathbf{L}_3$)	*1.7*	*1.3*	*2.3*	*4.3*	*4.8*	*3.5*
	PLSQR($\mathbf{L}_4$)	(1.6)	(1.8)	(2.2)	(4.8)	(5.8)	(7.4)
1/2m&1/4a	LSQR($\mathbf{L}_1$)	16.7	17.3	23.5	23.7	27.5	27.3
	PLSQR($\mathbf{L}_2$)	5.0	5.4	8.1	7.6	8.8	9.1
	PLSQR($\mathbf{L}_3$)	*4.8*	*4.8*	*9.3*	*9.7*	*11.1*	*10.5*
	PLSQR($\mathbf{L}_4$)	(6.7)	(6.0)	(24.4)	(18.0)	(28.1)	(24.2)
1/4m&1/2m&1/4a	LSQR($\mathbf{L}_1$)	15.6	14.5	21.4	21.2	26.2	24.4
	PLSQR($\mathbf{L}_2$)	2.7	4.0	7.2	6.0	8.0	8.5
	PLSQR($\mathbf{L}_3$)	*2.8*	*3.9*	*6.9*	*8.0*	*12.4*	*10.4*
	PLSQR($\mathbf{L}_4$)	(4.0)	(3.9)	(10.2)	(14.6)	(15.7)	(20.2)
1/2m&1/4a&1/2a	LSQR($\mathbf{L}_1$)	8.0	3.2	14.2	11.4	17.7	18.9
	PLSQR($\mathbf{L}_2$)	1.3	1.1	3.2	3.0	8.8	9.1
	PLSQR($\mathbf{L}_3$)	*1.4*	*1.0*	*2.9*	*3.4*	*5.7*	*5.9*
	PLSQR($\mathbf{L}_4$)	(1.7)	(1.7)	(3.1)	(3.5)	(5.7)	(5.7)

Note: Underlined RPE values are for PLSQR with bidiagonal matrix $\mathbf{L}_2$, italics RPE values are for PLSQR with tri-diagonal matrix $\mathbf{L}_3$, the RPE values in parentheses are for PLSQR with four diagonal matrix $\mathbf{L}_4$ and other values are for LSQR with identity matrix $\mathbf{L}_1$.

Table 1 tabulates the RPE values of LSQR and PLSQR with three different regularization matrices in 12 cases. When LSQR is adopted to identify the biaxial time-varying forces, the RPE values are less than 30% in 10 cases out of all 12 cases with 1%, 5% and 10% noise levels. Jacobsen and Hansen [35] pointed out that the regularization method is a good means of solving ill-posed problem. Preconditioned LSQR is a typical regularization approach by choosing proper regularization matrix to solve or to reduce the effects of ill-posedness on identification results.

When PLSQR($\mathbf{L}_2$), PLSQR($\mathbf{L}_3$) and PLSQR($\mathbf{L}_4$) are adopted to identify the biaxial time-varying forces, the RPE values are less than 30% in all 12 cases with three kinds of noise levels. Moreover, with the noise level increases, the RPE values of PLSQR only increase slightly owing to its strong robustness. As shown in the Fig.3 to Fig.5, the identification forces of PLSQR are very close to the true forces under various cases due to good adaptability with type of sensors and number of sensors. More importantly, the identification accuracy of

PLSQR is much better than LSQR when both front and rear axles are not simultaneously present on the beam, which means that the PLSQR has strong immunity of ill-posed problem.

Considering altogether the RPE values of PLSQR($\mathbf{L}_2$), PLSQR($\mathbf{L}_3$) and PLSQR($\mathbf{L}_4$) in all 12 cases, the RPE values of PLSQR($\mathbf{L}_3$) are relatively smaller than PLSQR($\mathbf{L}_2$) and PLSQR($\mathbf{L}_4$). Simultaneously, the matrix $\mathbf{L}_3$ is chosen as regularization matrix of PLSQR firstly, and then the calibration studies are carried out with static force, single axle force and other biaxial time-varying forces. All of the results show that the matrix $\mathbf{L}_3$of PLSQR has high identification accuracy and can be chosen as regularization matrix of PLSQR in MFI, which is case independent. Then the matrix $\mathbf{L}_3$ is chosen as the optimal regularization matrix of PLSQR and will be default adopted in subsequent studies. As mentioned above, the PLSQR is a hybrid method between a direct and an iterative regularization algorithm and the identification accuracy of PLSQR is influenced by the number of iterations. The optimal number of iterations is adopted in this study and will be examined in details in the next section.

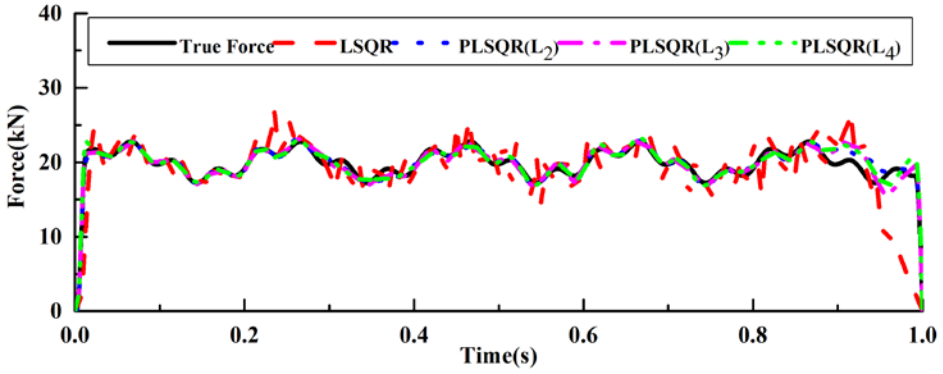

(a)

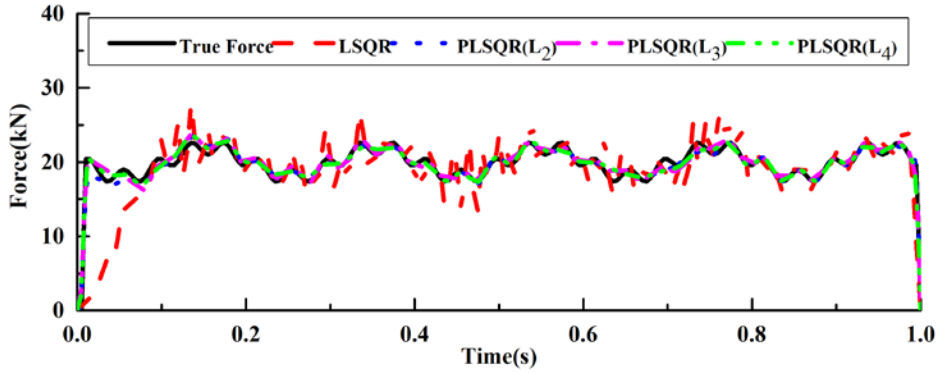

(b)

Fig.3. MFI from bending moment responses by LSQR and PLSQR with three regularization matrices (1/4m&1/2m&3/4m 1% Noise). (a) Front axle; (b) Rear axle.

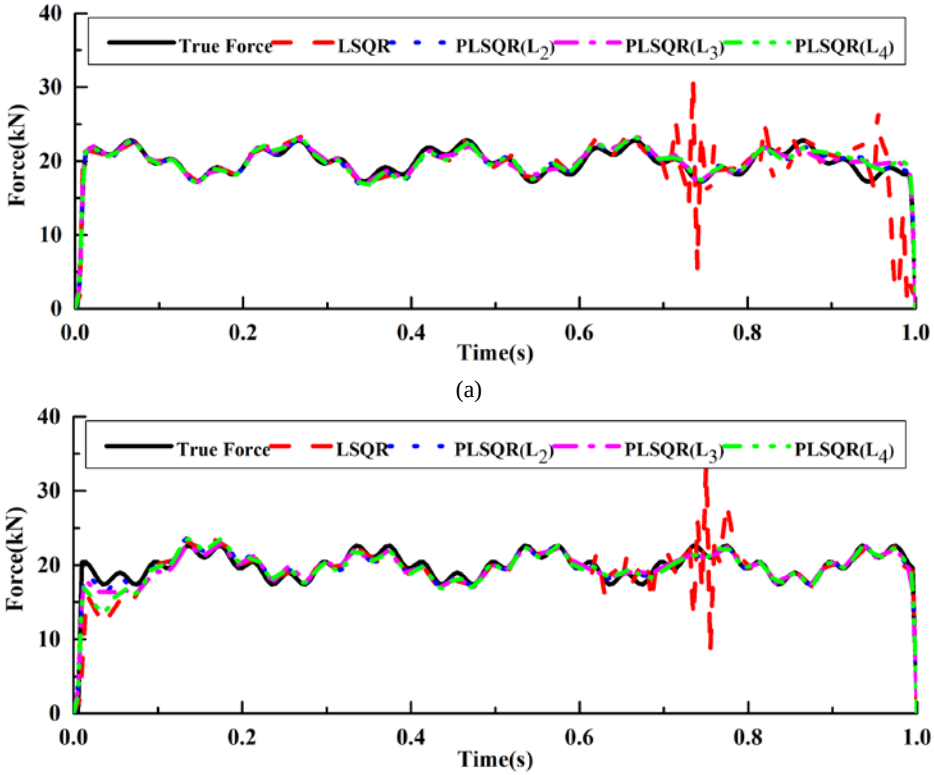

(a)

(b)

Fig.4. MFI from combined responses by LSQR and PLSQR with three regularization matrices (1/4m&1/2m&1/4a&1/2a 5% Noise). (a) Front axle; (b) Rear axle.

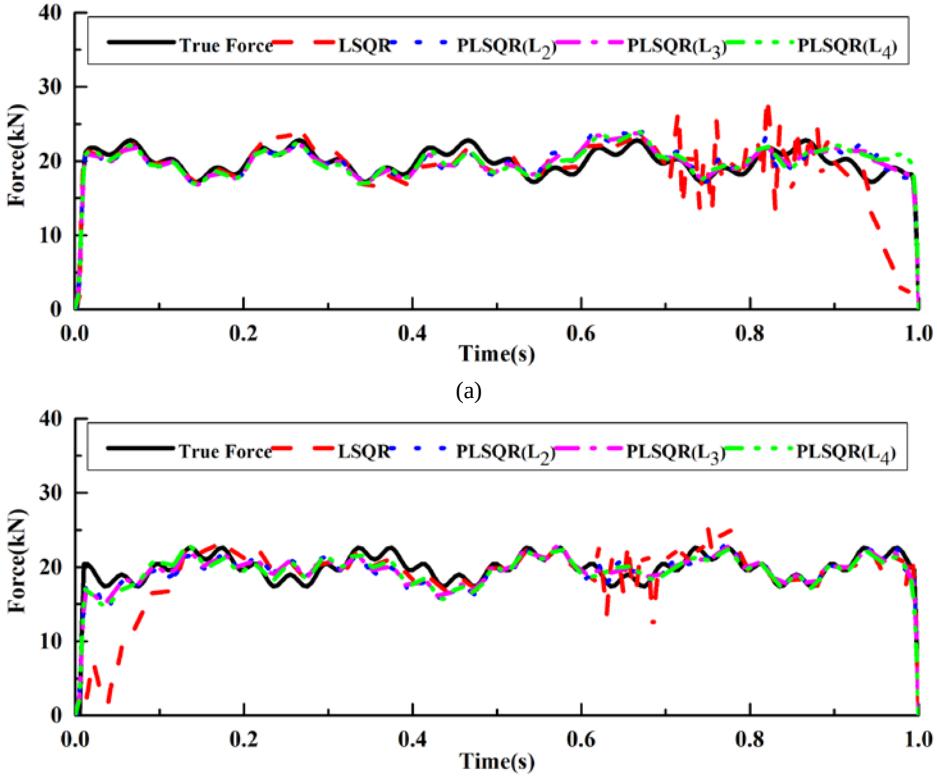

(a)

(b)

Fig.5. MFI from combined responses by LSQR and PLSQR with three regularization matrices (1/2m&1/4a&1/2a 10% Noise). (a) Front axle; (b) Rear axle.

3.3. Choosing optimal number of iterations j for PLSQR

As shown in the Fig.6, the RPE values of MFI from acceleration responses maintain less than 3% from 200 to 2000 with 1% noise level. It means that when the noise level is low it is not necessary to find optimal number of iteration because the calculation time and the identification cost outweigh the benefit. The efficacy of the optimal number of iterations when there is a high level of noise will be investigated further in this section. As shown in Table 2, the optimal number of iterations $j3$ is determined by RPE values compared identification force with true force. So there is obvious limitation without knowing the actual moving force. As shown in the Fig.6 to Fig.8, the effect of the number of iterations has similar behavior when acceleration responses contained in MFI. With increasing the number of iterations, the RPE values firstly increase rapidly and then decrease sharply, and then the RPE values keep a small fluctuation in the middle of the curve. When the number of iterations is selected close to 200, the RPE values are quite low in all cases as shown in the Fig.6 to Fig.9. The normal number of iterations $j4 = 200$ is therefore selected to compare with other number of iterations in the following studies.

As shown in the Fig.6 to Fig.8, the RPE values curve has a significant peak corresponding to abscissa values 20 and then the worst number of iterations $j2 = 20$ is selected to reveal the reasons. At the same time, the RPE values are still relatively small corresponding to very small abscissa values and then the minimum number of iterations $j1 = 1$ is selected to reveal the identification results of the PLSQR($\mathbf{L}_3$) with number of iterations only once.

As shown in the Fig.9, when moving force is identified from bending moment responses alone, the RPE values will exceed 100% when the number of iterations exceeds 1000 with 10% noise level. Therefore, choosing the optimal number of iterations has significant influence on the identification accuracy of the PLSQR.

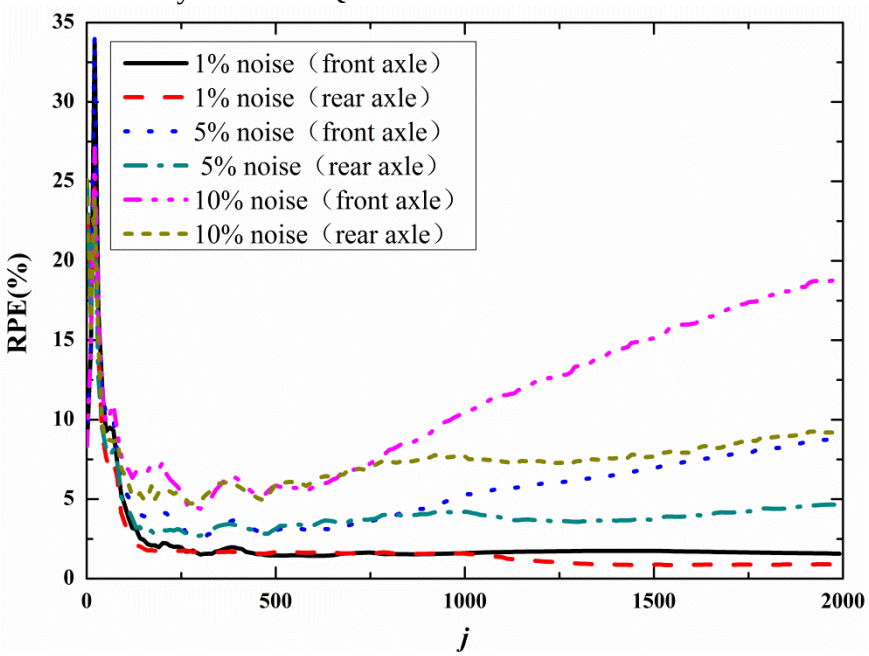

Fig.6. The RPE values of different number of iterations j in MFI by PLSQR from two acceleration responses (1/4a&1/2a)

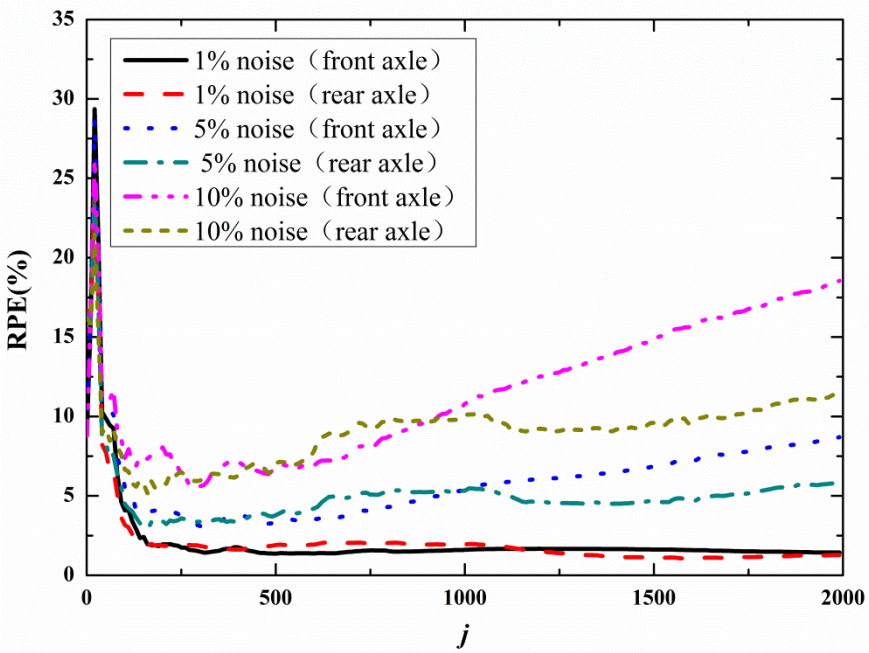

Fig.7. The RPE values of different number of iterations *j* in MFI by PLSQR from three combined responses (1/2m&1/4a&1/2a)

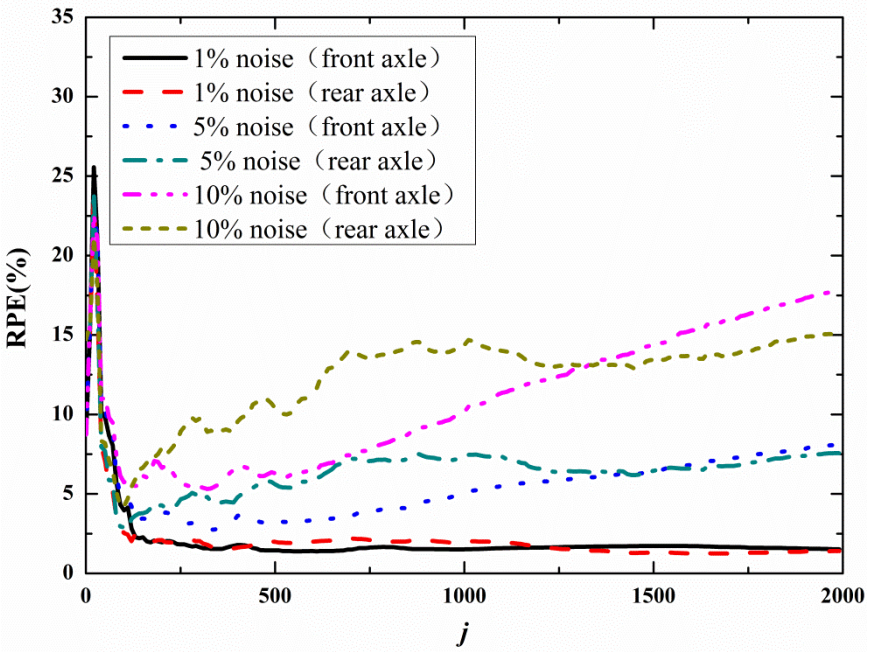

Fig.8. The RPE values of different number of iterations *j* in MFI by PLSQR from four combined responses (1/4m&1/2m&1/4a&1/2a)

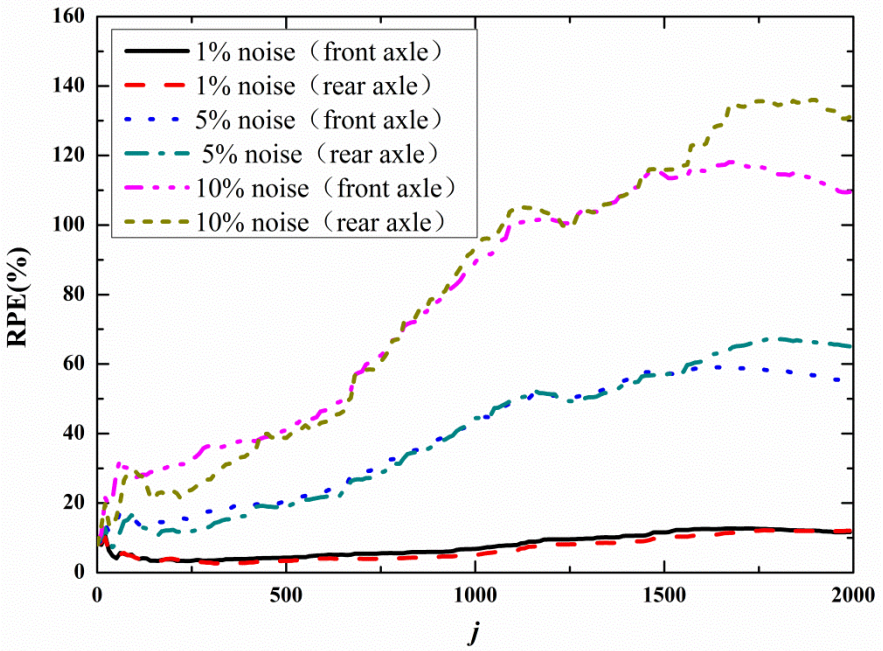

Fig.9. The RPE values of different number of iterations j in MFI by PLSQR from three bending moment responses (1/4m&1/2m&3/4m)

Table 2 tabulates the RPE values of PLSQR($\mathbf{L}_3$) with four different numbers of iterations in all 12 cases. The results show that the RPE values are less than 30% in all 12 cases and almost remain constant with noise level increasing when the minimum number of iterations $j1 = 1$ is selected. While as shown in the Fig.10 to Fig.12, the identification results are similar to the average load and cannot truly reflect the load fluctuations with number of iterations $j1 = 1$.

As shown in Fig.10 to Fig.12, the RPE values of PLSQR($\mathbf{L}_3$) become largest with number of iterations $j2 = 20$ due to the ill-posed problem, especially when both front and rear axles are not simultaneously present on the beam. Consequently, it is suggested that the number of $j2 = 20$ should be excluded in PLSQR($\mathbf{L}_3$).

When the optimal number of iterations $j3$ and the reasonable number of iterations $j4 = 200$ selected, both of the identification forces of the two kinds of number of iterations are very close to the true forces as shown in Table 2 and Fig.10 to Fig.12. It means that when the optimal number of iterations cannot be reasonably determined without knowing the actual moving force, the normal number of iterations $j4 = 200$ of PLSQR($\mathbf{L}_3$) can be selected to facilitate MFI.

Table 2
The RPE values (%) of PLSQR($\mathbf{L}_3$) with four different numbers of iterations

Sensor location	axle	1% noise				5% noise				10% noise			
		$j1$	$j2$	$j3$	$j4$	$j1$	$j2$	$j3$	$j4$	$j1$	$j2$	$j3$	$j4$
1/4m&1/2m	front	8.5	10.1	*4.6*	(5.3)	8.6	11.7	*17.6*	(23.2)	8.7	14.9	*25.7*	(48.4)
	rear	8.4	9.7	*4.1*	(5.0)	8.3	13.0	*9.9*	(22.9)	8.2	18.7	*19.2*	(48.3)
1/4m&1/2m&3/4m	front	8.6	10.7	*3.9*	(3.8)	8.7	13.9	*13.8*	(15.0)	8.9	21.7	*27.4*	(30.2)
	rear	8.2	10.2	*2.8*	(4.0)	8.2	12.8	*12.7*	(12.2)	8.1	19.9	*29.2*	(23.4)
1/4a&1/2a	front	8.5	25.7	*1.4*	(2.2)	8.4	25.2	*2.4*	(4.2)	8.3	24.6	*4.3*	(7.3)
	rear	25.0	31.8	*0.9*	(1.8)	25.1	31.4	*2.7*	(3.1)	25.1	30.8	*4.7*	(5.7)
1/4a&1/2a&3/4a	front	8.7	26.2	*0.7*	(0.9)	8.8	25.1	*1.5*	(1.8)	8.8	23.8	*2.7*	(2.9)

1/2m&1/2a	rear	26.8	25.9	*0.9*	(1.8)	26.8	25.4	*2.5*	(2.6)	26.9	24.9	*3.9*	(4.4)
	front	9.0	29.9	*3.2*	(3.4)	8.9	33.7	*10.2*	(10.5)	8.7	35.0	*14.9*	(21.4)
1/4m&1/2m&1/2a	rear	13.4	30.9	*3.5*	(3.6)	13.1	30.0	*7.4*	(10.8)	12.8	30.7	*9.5*	(21.5)
	front	8.7	30.2	*2.6*	(3.5)	8.7	30.4	*8.0*	(8.2)	8.6	30.8	*15.2*	(16.5)
1/4m&1/2m&1/4a&1/2a	rear	12.1	29.5	*2.6*	(3.0)	12.0	29.3	*9.6*	(11.4)	11.9	31.0	*9.1*	(23.5)
	front	8.9	23.0	*1.6*	(1.9)	8.8	22.3	*3.1*	(3.7)	8.7	21.6	*5.1*	(6.7)
1/4m&1/4a	rear	15.1	24.7	*1.3*	(2.1)	14.9	24.3	*3.7*	(4.2)	14.8	24.0	*5.9*	(7.9)
	front	9.1	24.9	*4.7*	(9.4)	9.0	23.0	*9.7*	(18.4)	8.9	20.8	*10.2*	(33.7)
1/4m&1/4a&1/2a	rear	17.8	24.2	*4.7*	(5.9)	17.9	23.7	*7.1*	(14.3)	18.1	23.1	*7.6*	(27.0)
	front	9.1	26.9	*1.7*	(1.9)	9.1	26.5	*2.3*	(3.2)	9.0	26.1	*4.8*	(5.8)
1/2m&1/4a	rear	19.0	27.1	*1.3*	(2.1)	19.0	26.7	*4.3*	(4.2)	19.1	26.2	*3.5*	(8.1)
	front	9.0	31.4	*4.8*	(8.2)	8.8	29.0	*9.3*	(17.0)	8.6	26.4	*11.1*	(34.3)
1/4m&1/2m&1/4a	rear	14.8	26.6	*4.8*	(6.1)	14.5	25.0	*9.7*	(14.6)	14.1	23.2	*10.5*	(29.6)
	front	8.8	25.8	*2.8*	(7.4)	8.7	25.4	*6.9*	(7.0)	8.7	25.4	*12.4*	(13.2)
1/2m&1/4a&1/2a	rear	13.2	23.5	*3.9*	(4.0)	13.0	24.3	*8.0*	(8.2)	12.8	25.7	*10.4*	(17.2)
	front	9.1	24.7	*1.4*	(1.9)	9.0	24.0	*2.9*	(4.3)	8.8	23.2	*5.7*	(8.0)
	rear	16.7	27.8	*1.0*	(2.0)	16.4	27.1	*3.4*	(3.3)	16.2	26.1	*5.9*	(6.2)

Note: Underlined RPE values are for PLSQR($\mathbf{L}_3$) with the worst number of iterations $j2 = 20$, italics RPE values are for PLSQR($\mathbf{L}_3$) with the optimal number of iterations $j3$, the RPE values in parentheses are for PLSQR($\mathbf{L}_3$) with normal number of iterations $j4 = 200$ and other RPE values are for PLSQR($\mathbf{L}_3$) with the minimum number of iterations $j1 = 1$.

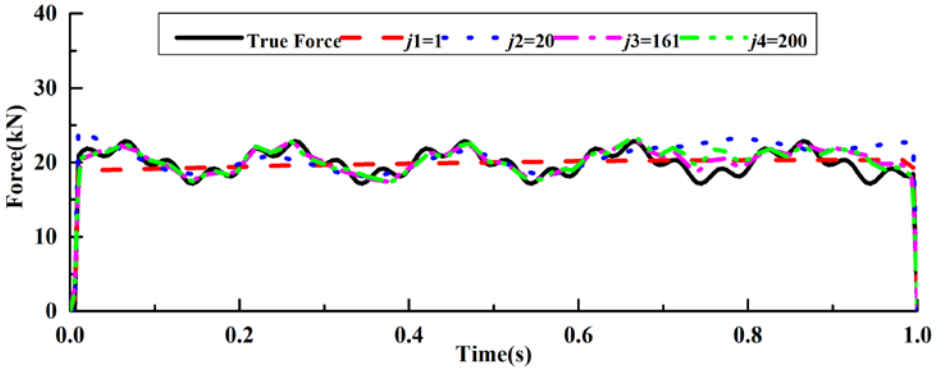

(a)

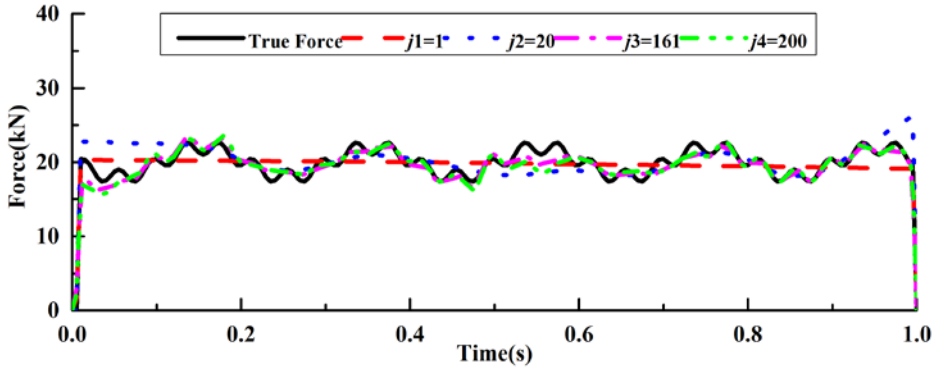

(b)

Fig.10. MFI from bending moment responses by PLSQR with four different numbers of iterations j (1/4m&1/2m 1% Noise). (a) Front axle; (b) Rear axle.

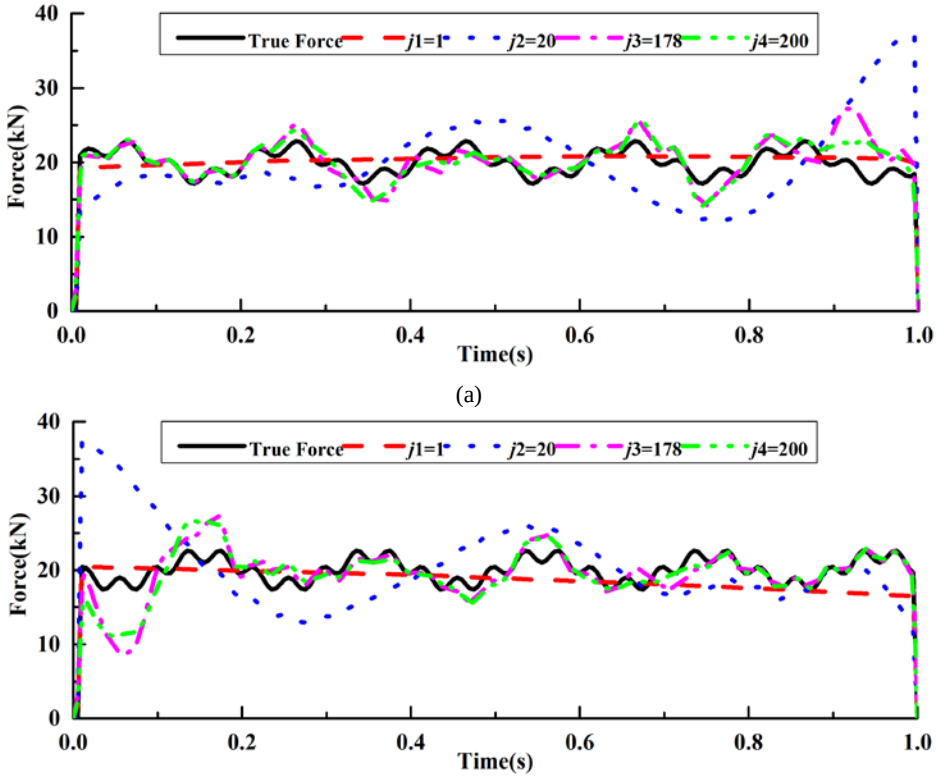

(a)

(b)

Fig.11. MFI from combined responses by PLSQR with four different numbers of iterations *j* (1/4m&1/2m&1/2a 5% Noise). (a) Front axle; (b) Rear axle.

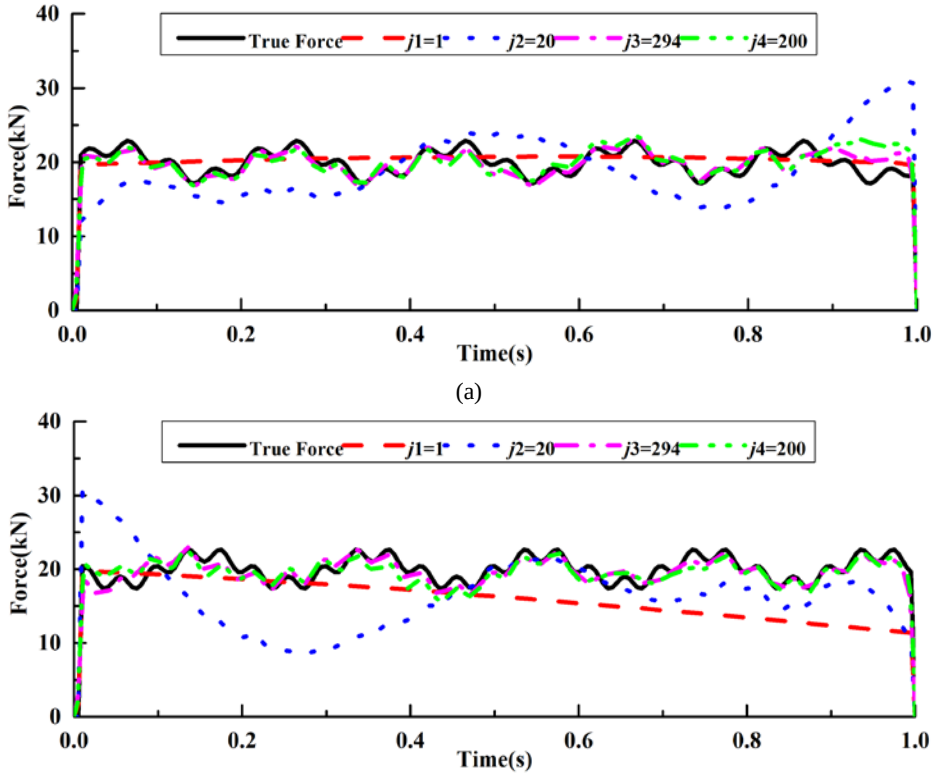

(a)

(b)

Fig.12. MFI from acceleration responses by PLSQR with four different numbers of iterations *j* (1/4a&1/2a 10% Noise). (a) Front axle; (b) Rear axle.

3.4. PLSQR versus TDM and the effect of vehicle speed on *PLSQR*

Former part of this study shows that all of the PLSQR($\mathbf{L}_2$), PLSQR($\mathbf{L}_3$) and PLSQR($\mathbf{L}_4$) have strong robustness to responses noise and ill-posedness problem. Then the identification ability of PLSQR will be compared with the TDM in this part. The illustration results of Fig.13 show that MFI from bending moment responses alone by TDM suffers from large fluctuation even with only one percent noise level added. When combined responses from two sensors are used, the accuracy of TDM is also unacceptable as shown in Fig.14. Only when three acceleration responses used alone, the identification accuracy of TDM is improved being similar to that of PLSQR as shown in Fig.15. It means that the TDM is sensitive to both the type of sensors and the number of sensors; the identification results will unacceptable when bending moment measurements are used alone or the number of sensors is small.

Comparing with TDM, the biaxial moving forces identified by PLSQR($\mathbf{L}_2$), PLSQR($\mathbf{L}_3$) and PLSQR($\mathbf{L}_4$) are very close to the true forces in all cases as shown in Fig.13 to Fig.15. The PLSQR has excellent adaptability with both the type of sensors and the number of sensors. The numerical simulation results also show that the accuracy and acceptability of identification forces by PLSQR will improve with more acceleration responses and lower disturbance noise. In order to facilitate the economical application of the PLSQR in field tests, specific sensor requirements are suggested as follows. When noise level is less than 5%, at least two responses are measured and at least one acceleration response is included. When noise level is higher than 5%, at least three responses are measured and at least two acceleration responses are included.

As the moving speed is an important factor affecting in MFI, the effect of the moving speed on PLSQR($\mathbf{L}_3$) is simulated with three decreasing moving speeds, namely $c_1 = 40\mathrm{m} \cdot \mathrm{s}^{-1}$, $c_2 = 30\mathrm{m} \cdot \mathrm{s}^{-1}$ and $c_3 = 20\mathrm{m} \cdot \mathrm{s}^{-1}$, respectively. The time for passing over the bridge corresponding to these three speeds is 1s, $\frac{4}{3}$s and 2s, respectively. Due to the consistency rule of the effect of vehicle speed on PLSQR($\mathbf{L}_3$), Table 3 tabulates four representative cases from all 12 cases. The simulation results show that the identification accuracy is slightly improved and the optimal number of iterations is increased with the decrease of the speed. Similar to the normal number of iterations $j4 = 200$ of PLSQR($\mathbf{L}_3$) can be selected to facilitate MFI with speed c_1, the normal number of iterations $j = 220$ and $j = 300$ can be selected to facilitate MFI corresponding to speed c_2 and speed c_3, respectively.

As shown in Fig.16 and Fig.17, the biaxial moving forces identified by PLSQR($\mathbf{L}_3$) are very close to the true forces during the vehicle crosses the bridge with all three speeds. The illustration results show that the identification accuracy of PLSQR remains at a high level with different moving speeds, which is very beneficial for the application of PLSQR method in field trials.

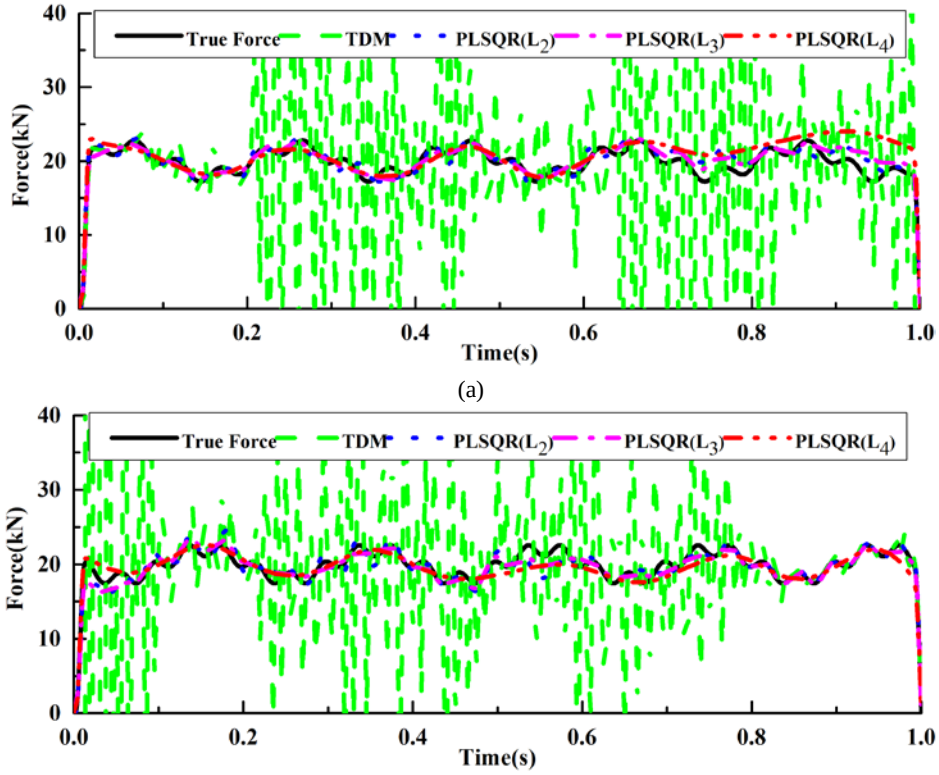

(a)

(b)

Fig.13. MFI by PLSQR and TDM from two bending moment responses (1/4m&1/2m 1% Noise). (a) Front axle; (b) Rear axle.

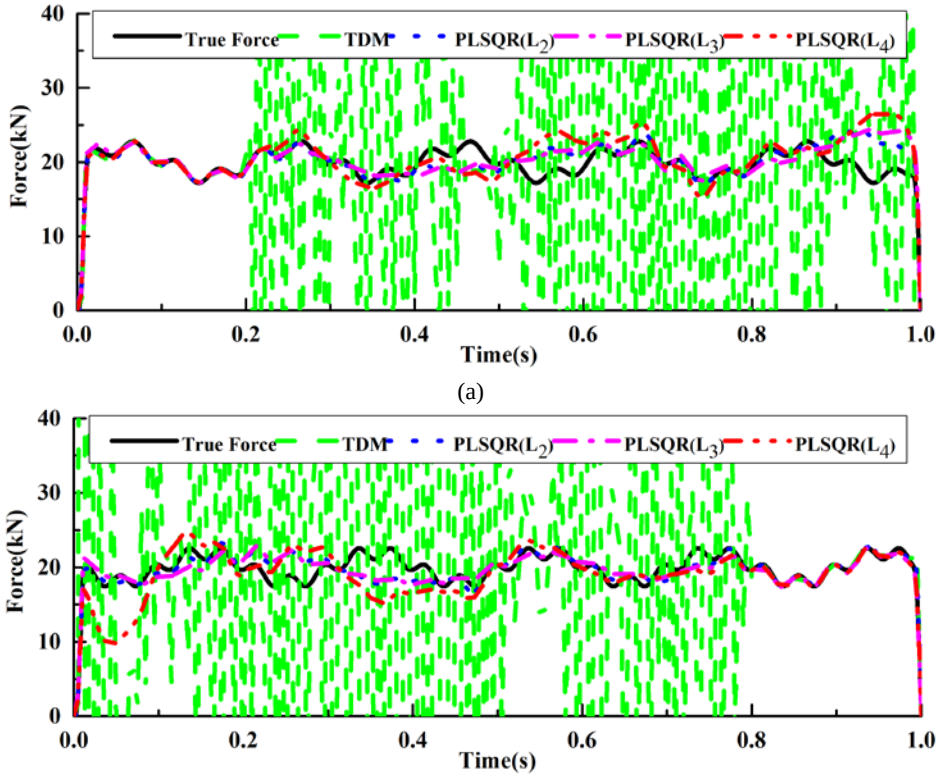

(a)

(b)

Fig.14. MFI by PLSQR and TDM from two combined responses (1/2m&1/2a 5% Noise). (a) Front axle; (b) Rear axle.

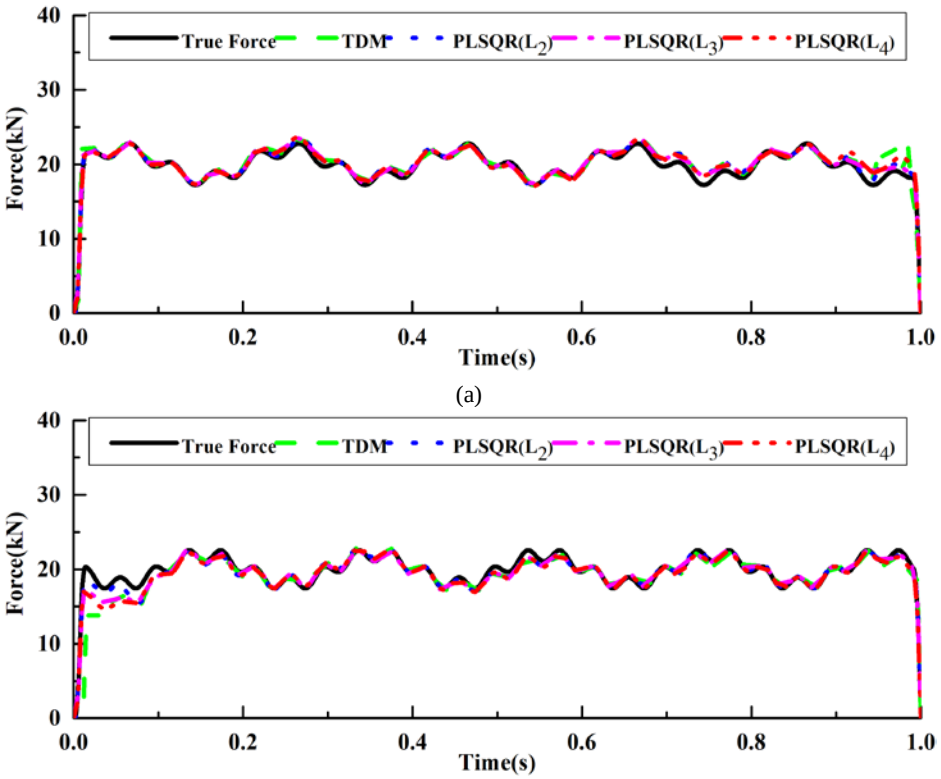

(a)

(b)

Fig.15. MFI by PLSQR and TDM from three acceleration responses (1/4a&1/2a&3/4a 10% Noise). (a) Front axle; (b) Rear axle.

Table 3
The RPE values (%) of PLSQR($\mathbf{L}_3$) with three different moving speeds

Sensor location	axle	1% noise			5% noise			10% noise		
		c_1	c_2	c_3	c_1	c_2	c_3	c_1	c_2	c_3
1/4m&1/2m&3/4m	front	*3.9*	2.7	2.7	*13.8*	9.3	7.3	*27.4*	23.3	19.9
	rear	*2.8*	3.2	2.7	*12.7*	10.6	6.8	*29.2*	29.0	20.8
1/4m&1/2m&1/4a&1/2a	front	*1.6*	1.6	1.5	*3.1*	2.7	2.6	*5.1*	4.1	4.1
	rear	*1.3*	1.3	1.3	*3.7*	3.3	2.2	*5.9*	5.2	3.1
1/4m&1/4a&1/2a	front	*1.7*	1.6	1.5	*2.3*	2.7	2.7	*4.8*	4.2	4.0
	rear	*1.3*	1.3	1.3	*4.3*	2.7	2.4	*3.5*	3.7	3.0
1/2m&1/4a&1/2a	front	*1.4*	1.4	1.3	*2.9*	3.0	3.0	*5.7*	4.4	4.3
	rear	*1.0*	1.0	1.0	*3.4*	3.2	2.4	*5.9*	4.8	3.4

Note: Italics RPE values are for PLSQR($\mathbf{L}_3$) with the moving speed $c_1 = 40\mathrm{m}\cdot\mathrm{s}^{-1}$, underlined RPE values are for PLSQR($\mathbf{L}_3$) with the moving speed $c_2 = 30\mathrm{m}\cdot\mathrm{s}^{-1}$ and other RPE values are for PLSQR($\mathbf{L}_3$) with the moving speed $c_3 = 20\mathrm{m}\cdot\mathrm{s}^{-1}$.

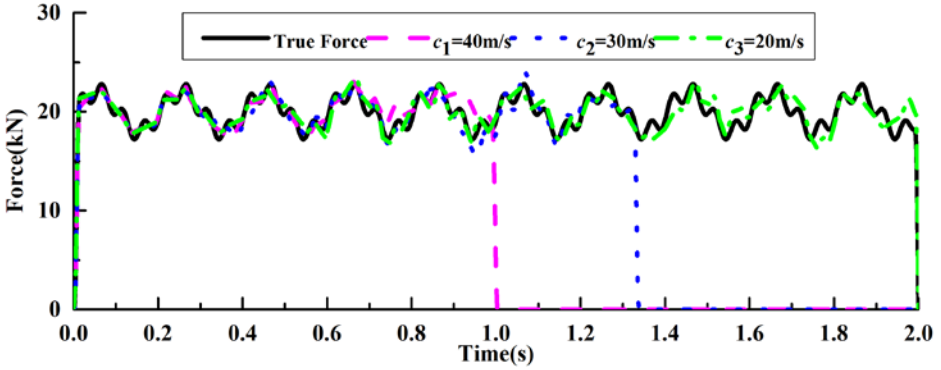

(a)

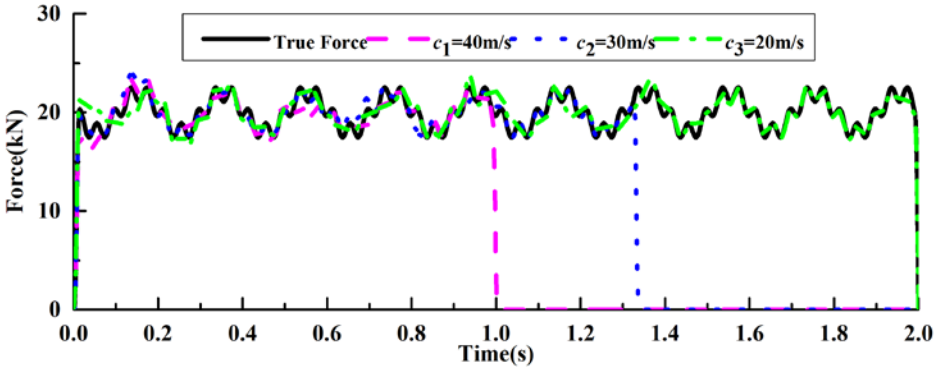

(b)

Fig.16. MFI with three different speeds by PLSQR($\mathbf{L}_3$) from acceleration responses (1/4m&1/2m 1% Noise). (a) Front axle; (b) Rear axle.

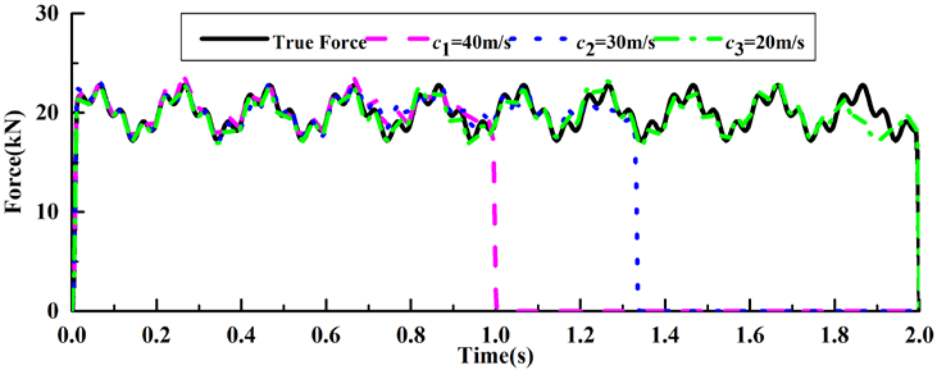

(a)

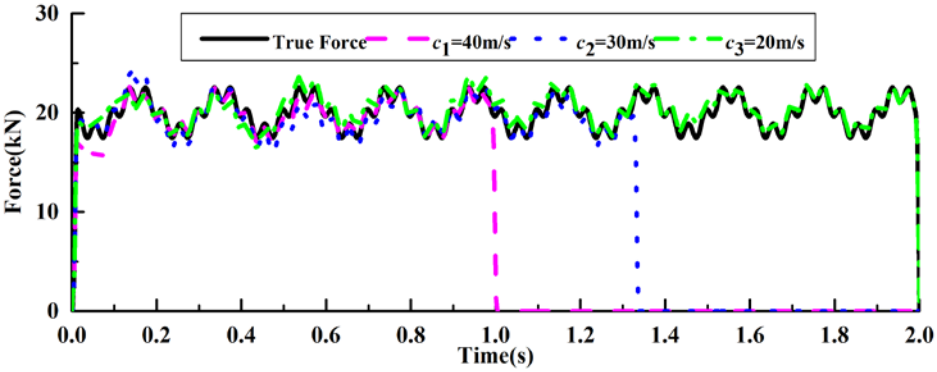

(b)

Fig.17. MFI with three different speeds by PLSQR($\mathbf{L}_3$) from acceleration responses (1/4a&1/2a&3/4a 10% Noise). (a) Front axle; (b) Rear axle.

4. Conclusions

In this work, a PLSQR method is proposed to identify moving force by preconditioning LSQR. By means of numerical simulations, a comprehensive parametric study has been done and the following conclusions can be drawn:

(1) When PLSQR($\mathbf{L}_2$), PLSQR($\mathbf{L}_3$) and PLSQR($\mathbf{L}_4$) are adopted to identify the moving force, the identification accuracy in all 12 cases is significantly improved compared with LSQR($\mathbf{L}_1$). The PLSQR has overcome the ill-posed problem by choosing proper regularization matrix. In addition, the RPE values of PLSQR($\mathbf{L}_3$) are relatively smaller than

PLSQR($\mathbf{L}_2$) and PLSQR($\mathbf{L}_4$) as mentioned above. Then the matrix $\mathbf{L}_3$ is selected as the optimal regularization matrix for preconditioning LSQR.

(2) When the optimal number of iterations $j3$ and the reasonable number of iterations $j4 = 200$ selected, both of the identification forces of the two kinds of number of iterations are very close to the true forces as shown previously. It means that when the optimal number of iterations cannot be determined without knowing the actual moving force, the normal number of iterations $j4 = 200$ of PLSQR($\mathbf{L}_3$) can be selected which also meet the requirements of MFI. On the contrary, the number of iterations $j1 = 1$ and $j2 = 20$ of PLSQR($\mathbf{L}_3$) should be avoided as the former cannot truly reflect the load fluctuations and the latter amplify the ill-posed problem.

(3) Comparing with TDM, the identification accuracy of PLSQR is much higher in all cases. The PLSQR has excellent adaptability with both the type of sensors and the number of sensors, it also has strong noise immunity and robust with ill-posed problem. Moreover, the identification accuracy is slightly improved with the decrease of the speed. The illustrated results show that the identification accuracy of PLSQR($\mathbf{L}_3$) remains at a very high level with different moving speeds, which highlights the robustness of PLSQR method in field tests.

Finally, it is noted that, compared with the situations that both of the axles are running on the bridge, the identification accuracy of PLSQR is still lower when only either the front or rear axle is on the bridge. It is therefore suggested that MFI through PLSQR not be performed during these situations, and this problem will be investigated further in future works of the present authors. In addition, further studies about the independent of regularization matrix selecting and the improvement of identification efficiency without sacrificing the identification accuracy will also be discussed in the next paper.

Acknowledgments

This research was supported by Key Science and Technology Program of Henan Province, China (Grant Number 192102310011), MOE Key Lab of Disaster Forecast and Control in Engineering, Jinan University (Grant Number 20180930003) and National Natural Science Foundation of China (Grant Numbers 51678278 and 51278226).

References:

[1] M. Lydon, S.E. Taylor, D. Robinson, A. Mufti, E.J.O. Brien. Recent developments in bridge weigh in motion (B-WIM), J. Civil Struct. Health Monit. 6 (2016) 69-81.
[2] J. Sanchez, H. Benaroya, Review of force reconstruction techniques, J. Sound Vib. 333 (2014) 2999-3018.
[3] C. O'Connor, T.H.T. Chan, Dynamic wheel loads from bridge strains, Eng. Struct. 114 (1988) 1703-1723.
[4] S.S. Law, T.H.T. Chan, Q.H. Zeng, Moving force identification: a time domain method, J. Sound Vib. 201(1) (1997) l-22.
[5] T.H.T. Chan, S.S. Law, T.H. Yung, X.R. Yuan, An interpretive method for moving force identification, J. Sound Vib. 219 (1999) 503-524.
[6] S.S. Law, T.H.T. Chan, Q.H. Zeng, Moving force identification-a frequency and time domains analysis, J. Dyn. Sys. Meas. Control ASME 121 (1999) 394-401.
[7] L. Yu, T.H.T. Chan, Recent research on identification of moving loads on bridges, J. Sound Vib. 305 (2007) 3-21.

[8] X.Q. Zhu, S.S. Law, Identification of vehicle axle loads from bridge dynamic responses, J. Sound Vib. 236 (2000) 705-724.
[9] X.Q. Zhu, S.S. Law, Identification of moving interaction forces with incomplete velocity information, Mech. Syst. Signal Process. 17 (2003) 1349-1366.
[10] X.Q. Zhu, S.S. Law, Moving load identification on multi-span continuous bridges with elastic bearings, Mech. Syst. Signal Process. 20 (2006) 1759-1782.
[11] T.H.T. Chan, D.B. Ashebo, Theoretical study of moving force identification on continuous bridges, J. Sound Vib. 295 (2006) 870-883.
[12] L. Yu, T.H.T. Chan, J.H. Zhu, A MOM-based algorithm for moving force identification: Part I - Theory and numerical simulation, Struct. Eng. Mech. 29 (2008) 135-154.
[13] Y. Yu, C.S. Cai, L. Deng, State-of-the-art review on bridge weigh-in-motion technology, Adv. Struct. Eng. 19 (2016) 1514-1530.
[14] J. Dowling, E.J. Obrien, A. González, Adaptation of cross entropy optimization to a dynamic bridge WIM calibration problem, Eng. Struct. 44 (2012) 13-22.
[15] A. Berry, O. Robin, F. Pierron, Identification of dynamic loading on a bending plate using the virtual fields method, J. Sound Vib. 333 (2014) 7151-7164.
[16] Z. Li, Z.P. Feng, F.L. Chu, A load identification method based on wavelet multi-resolution analysis, J. Sound Vib. 333 (2014) 381-391.
[17] T. Pinkaew, Identification of vehicle axle loads from bridge responses using updated static component technique, Eng. Struct. 28 (2006) 1599-1608.
[18] A. González, C. Rowley, E.J. Obrien, A general solution to the identification of moving vehicle forces on a bridge, Int. J. Numer. Methods Eng. 75 (2008) 335-354.
[19] Y.M. Mao, X.L. Guo, Y. Zhao, A state space force identification method based on Markov parameters precise computation and regularization technique, J. Sound Vib. 329 (2010) 3008-3019.
[20] H. Ronasi, H. Johansson, F. Larsson, A numerical framework for load identification and regularization with application to rolling disc problem, Comput. Struct. 89 (2011) 38-47.
[21] S.Q. Wu, S.S. Law, Moving force identification based on stochastic finite element model, Eng. Struct. 32 (2010) 1016-1027.
[22] Y. Ding, S.S. Law, Structural damping identification based on an iterative regularization method, J. Sound Vib. 330 (2011) 2281-2298.
[23] J. Li, S.S. Law, H. Hao, Improved damage identification in bridge structures subject to moving loads: numerical and experimental studies, Int. J. Mech. Sci. 74 (2013) 99-111.
[24] Y. Ding, S.S. Law, B. Wu, G.S. Xu, Q. Lin, H.B. Jiang, Q.S. Miao, Average acceleration discrete algorithm for force identification in state space, Eng. Struct. 56 (2013) 1880-1892.
[25] D.M. Feng, H. Sun, M.Q. Feng, Simultaneous identification of bridge structural parameters and vehicle loads, Comput. Struct. 157 (2015) 76-88.
[26] B.J. Qiao, X.F.Chen, X.F.Xue, X.J.Luo, R.N.Liu, The application of cubic B-spline collocation method in impact force identification, Mech. Syst. Signal Process. 64-65 (2015) 413-427.
[27] B.J. Qiao, X.W. Zhang, X.J. Luo, X.F. Chen, A Force identification method using cubic b-spline scaling functions, J. Sound Vib. 337 (2015) 28-44.
[28] J. Liu, X.S. Sun, X. Han, A novel computational inverse technique for load identification using the shape function method of moving least square fitting, Comput. Struct. 144 (2014) 127-137.
[29] X.S. Sun, J. Liu, X. Han, A new improved regularization method for load identification, Inverse Probl. Sci. Eng. 22(2014) 1602-1076.
[30] J. Liu, X.S. Sun, X. Han, Dynamic load identification for stochastic structures based on Gegenbauer polynomial approximation and regularization method, Mech. Syst. Signal Process. 56-57 (2015) 35-54.
[31] J. Liu, X.H. Meng, C. Jiang, X. Han, D.Q. Zhang, Time-domain Galerkin method for dynamic load identification, Int. J. Numer. Methods Eng. 105 (2016) 620-640.
[32] C.C. Paige, M.A. Saunders, LSQR: An algorithm for sparse linear equations and sparse least squares, ACM T. Math. Software 8 (1982) 43-71.
[33] M.A. Saunders, Solution of sparse rectangular systems using LSQR and CRAIG, BIT Numer. Math. 35 (1995) 588-604.
[34] S.J. Benbow, Solving generalized least-squares problems with LSQR, SIAM J. Matrix Anal. Appl. 21 (1999) 166-177.
[35] M. Jacobsen, P.C. Hansen, M.A. Saunders, Subspace preconditioned LSQR for discrete ill-posed problems, BIT Numer. Math. 43 (2003) 975-989.
[36] L. Reichel, Q. Ye, A generalized LSQR algorithm, Numer. Linear Algebra Appl. 15 (2008) 643-660.
[37] J. Baglama, L. Reichel, D. Richmond, An augmented LSQR method, Numer. Algorithms 64 (2013) 263-293.
[38] S. Karimi, B. Zali, The block preconditioned LSQR and GL-LSQR algorithms for the block partitioned matrices, Appl. Math. Comput. 227 (2014) 811-820.
[39] S.R. Arridge, M.M. Betcke, L. Harhanen, Iterated preconditioned LSQR method for inverse problems on unstructured grids, Inverse Probl. 30 (2014) 075009.